Deactivation of Copper Catalysts During CO_2 Reduction Occurs via Dissolution and Selective Redeposition Mechanism

Blaž Tomc,[a] Marjan Bele,[a] Mohammed Azeezulla Nazrulla,[a], [b] Primož Šket,[c] Matjaž Finšgar,[d] Angelja Kjara Surca,[a] Ana Rebeka Kamšek,[a], [e] Martin Šala,[f] Nejc Hodnik*[a], [g]

[a] B. Tomc, Dr. M. Bele, Dr. M. A. Nazrulla, Dr. A. K. Surca, A.R. Kamšek, Assoc. Prof. Dr. N. Hodnik
Department of Materials Chemistry, Laboratory for Electrocatalysis
National Institute of Chemistry
Ljubljana 1000, Slovenia
E-mail: Nejc.Hodniki@ki.si

[b] Dr. M. A. Nazrulla
Department of Chemistry
Manipal Institute of Technology, Manipal Academy of Higher Education
Manipal, Karnataka 576104, India

[c] Dr. P. Šket
Slovenian NMR centre
National Institute of Chemistry
Ljubljana 1000, Slovenia

[d] Assoc. Prof. Dr. M. Finšgar
Laboratory of Analytical Chemistry and Industrial Analysis
Faculty of Chemistry and Chemical Technology, University of Maribor
Maribor 2000, Slovenia

[f] A. R. Kamšek
Faculty of Chemistry and Chemical Technology, University of Ljubljana
Ljubljana 1000, Slovenia

[f] Dr. M. Šala
Department of Analytical Chemistry
National Institute of Chemistry
Ljubljana 1000, Slovenia

[g] Assoc. Prof. Dr. N. Hodnik
University of Nova Gorica
Nova Gorica 5000, Slovenia

Supporting information for this article is given via a link at the end of the document.

Abstract: As electrochemical CO_2 reduction (ECR) approaches industrialisation levels, addressing the challenge of uncontrolled restructuring and deactivation of copper (Cu) catalysts during operation is essential for the regulation of this phenomenon. Two different catalysts were prepared, each showing distinct changes in ECR products selectivity over prolonged operation. The detection of dissolved Cu species during electrolysis confirms the intermediates mediated Cu^0(s) dissolution mechanism at ECR potential, namely -0.8 to -1.1 V vs. reversible hydrogen electrode. A dynamic equilibrium between dissolution and subsequent redeposition leads to morphological restructuring. Additionally, our findings suggest that the electrodeposition of dissolved Cu species is biased towards less active sites due to their lower coverage by reaction intermediates such as adsorbed CO. The iterative cycles of the dissolution-redeposition mechanism at ECR potential lead to the growth of the less-active Cu surface at the cost of the more-active one. This gradual yet persistent restructuring mechanism consequently shifts selectivity away from ECR and towards hydrogen production. Both catalysts exhibited this general behaviour, although at different rates.

Introduction

The increasing concentration of CO_2 in Earth's atmosphere[1] has emerged as an urgent global concern due to its role in climate change and global warming. In response to this environmental challenge, a growing interest is in developing sustainable and efficient methods to capture and utilise CO_2.[2–4] ECR has gained considerable attention to not only reduce CO_2 emissions but also yield valuable chemicals and fuels from it. Utilising this reaction our reliance on fossil fuels could be mitigated, fostering the evolution of a circular and environmentally sustainable economy.

Cu-based catalysts have demonstrated a notable ability to electrochemically reduce CO_2 to high-value and energy-dense products, such as ethylene. The uniqueness of Cu as an ECR catalyst has been explained by the fact that it is the only metal with negative adsorption energy for CO, a key intermediate in ECR, and positive adsorption energy for H^+, an intermediate in the parasitic hydrogen evolution reaction (HER). This distinctive characteristic increases the longevity of adsorbed CO (*CO), thereby enhancing the probability of C-C coupling and generating desired C_{2+} products.[5–8] Although promising, the integration of Cu as an ECR electrocatalyst encounters notable hurdles, especially stemming from the intricate interplay within various parameters. Among these, catalyst morphology stands out as particularly important since it impacts both the activity and selectivity of ECR.[5,8–10] For example, cubic nanoparticles demonstrate better selectivity for ethylene compared to their spherical and octahedral counterparts,[5,10] and activity is significantly influenced by the size of the nanoparticles, with smaller ones tending to promote HER.[11] At the same time, commercial applications of ECR demand a catalyst with high faradaic efficiency (FE) and current density for a specific product and, of equal importance, long-term operational stability.[5,6]

The ECR protocol typically includes catalyst immersion in electrolyte without applied potential (later OCP; open circuit potential), during which the electrolyte becomes saturated with CO_2, followed by chronoamperometric (CA) measurement at a constant ECR potential, where the ECR commences. Numerous studies have provided substantial evidence of Cu surface restructuring at the initial stage of ECR protocol (OCP and the initiation of CA).[12–14] The dominant mechanism is dissolution-redeposition, occurring due to the presence of Cu-oxides on the catalyst surface.[15–18] This degradation process unfolds in two steps: firstly, the direct dissolution of Cu-oxides at OCP, followed by the subsequent electrodeposition onto the catalyst surface when ECR potential is applied at the start of CA. Dissolved Cu species are in the Cu^+ oxidation state.[19] Raaijman et al.[20] demonstrated that this initial restructuring can be limited if the catalyst gets exposed to the electrolyte under the influence of applied potential. Undissolved Cu-oxides undergo reduction to metallic Cu at the initiation of CA,[18,21] triggering transient dissolution followed by redeposition and, thus, some unavoidable restructuring.[17]

Nevertheless, mechanisms at the initial stage of ECR do not account for all Cu morphology alterations, as changes have been documented even at the CA during prolonged operation.[22–27] Vavra et al.[19] using density functional theory studies showed that soluble Cu species can exist at -1.2 V vs. reversible hydrogen electrode (RHE). They demonstrated that $[CuCO]^+_{3H2O}$, $[Cu_2CO_3]_{5H2O}$ and $[Cu_2C_2O_4]_{4H2O}$ exhibit negative formation energies at these conditions. Furthermore, they also suggested that the primary Cu dissolution pathway at ECR potential initiates through the formation of $[CuCO]^+_{3H2O}$ complex. Other studies also suggest that restructuring at ECR potential is facilitated by *CO.[21,28,29] Alterations were observed even in a CO atmosphere.[30]

Cu instability during the CA is of great importance, as it affects activity and selectivity, ultimately leading to its deactivation.[25] Herein, this study reveals the fundamental mechanisms of Cu catalysts restructuring and deactivation through a dynamic equilibrium between Cu dissolution and selective redeposition, intending to provide the understanding and, consequently, design principles for optimizing operational conditions and/or stable catalysts to effectively address these currently uncontrollable alterations.

Results and Discussion

To tackle the challenge of dynamic restructuring during the CA, the fundamentally similar dissolution-redeposition mechanism at the initial stage of the ECR protocol was thoroughly studied, observing the important factors in both Cu dissolution and electrodeposition. A catalyst demonstrating high Cu species dissolution at OCP was used (see Section S1 in Supporting Information). Identical location scanning electron microscopy (IL-SEM) was utilised to track Cu migration (Figure 1a,b). Dissolution at OCP occurred in two stages: (i) an initial rapid dissolution of Cu-oxides, followed by (ii) a slower process of metallic Cu oxidation with subsequent dissolution (Section S1). By applying the potential at the initiation of CA, the electrodeposition of dissolved Cu species led to the formation of spherical Cu nanoparticles ranging in size from 5 to 80 nm (Figure 1b and Section S1). This mechanism is schematically presented in Figure 1c,d. The primary products of the ECR were formate and ethylene (Section S2). Active Cu surface species were in the Cu^0 oxidation state (Section S3).

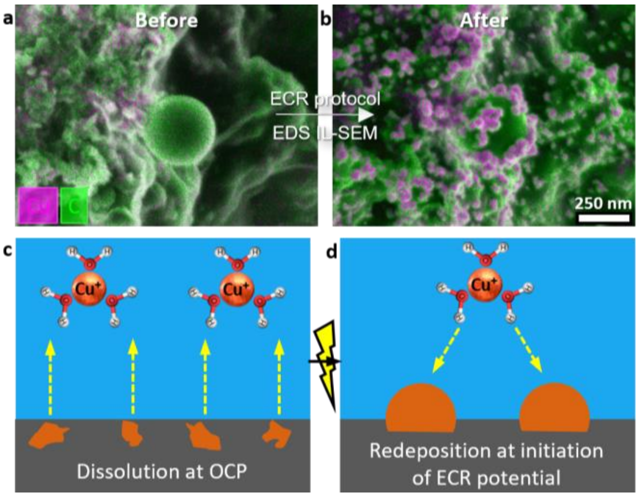

Figure 1. Energy dispersive X-ray spectroscopy (EDS) mapping overlay in association with IL-SEM of the catalyst a) before and b) after 25 minutes at OCP followed by the application of -0.975 V vs. RHE for 1 hour in CO_2-saturating 0.1 M $KHCO_3$. Schematic representation of c) the Cu nanoparticles dissolution at OCP and d) subsequent electrodeposition of dissolved Cu species when ECR potential was applied at the start of CA.

IL-SEM images demonstrated that the electrodeposition of Cu species and ECR are competing processes (Figure 2 and Section S6). When the catalyst, which was modified with ECR protocol as shown in Figure 1a,b andFigure **2**a,b, was subjected to a repeated ECR protocol at the potential of -0.975 V vs. RHE, the dissolution-redeposition mechanism led to the formation of new nanoparticles alongside pre-existing ones (Figure 2c,d). This contradicts the common Ostwald ripening mechanism principles, where larger particles exhibit uniform growth at the cost of smaller ones. On the other hand, when the experiment was repeated with argon purging instead of CO_2, Cu nanoparticles, marked in green, grew evenly at the cost of Cu nanoparticles, marked in red (Figure 2e,f). With CO_2 expected ECR activity and selectivity were observed (Section S2), while with argon, no products were detected.

The persistence of this intermediate on the surface facilitates C-C coupling, enabling the subsequent formation of desired C_{2+} products.[5–8] This process was optimal at around -1.0 V vs. RHE in terms of both activity and selectivity (Section S2), the potential at which the experiment in Figure 2c,d was conducted. The contradictions with Ostwald ripening arose because ECR commenced faster than the electrodeposition of dissolved Cu species. This led to the accumulation of adsorbed ECR intermediates on the Cu surface, blocking Cu electrodeposition. Consequently, Cu nanoparticles did not grow (some even shrunk), and only new Cu particles appeared in new regions (Figure 2d). In the control experiment where CO_2 was substituted with argon an Ostwald ripening occurred because the surface was not blocked by ECR intermediates. However, if the ECR was not optimal (e.g. -0.850 V vs. RHE), anisotropic Cu nanoparticles growth was observed (**Error! Reference source not found.** and **Error! Reference source not found.**). In these experiments, the Cu surface was only partially blocked with ECR intermediates.

Therefore, it can be concluded that ECR and electrodeposition of dissolved Cu species were competing reactions. The more optimal the ECR was, the better obstruction of the surface was achieved, even to the extent of complete blockage for electrodeposition. This is schematically presented in Figure 2g,h.

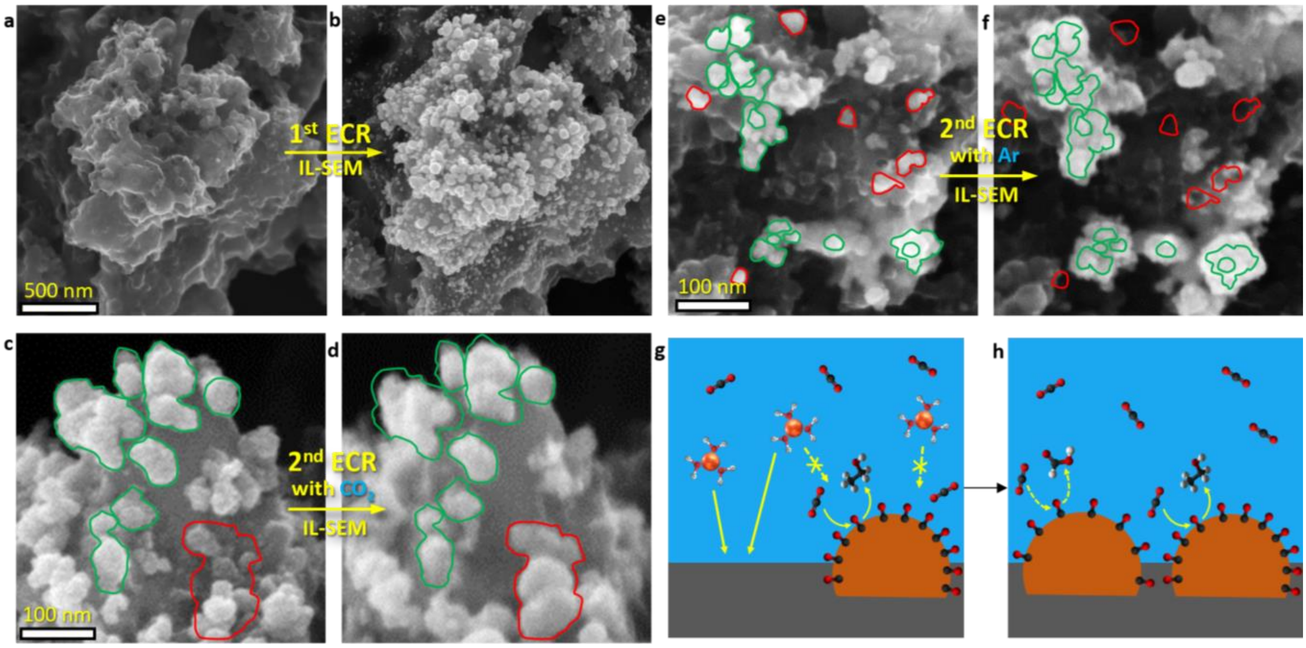

Figure 2. IL-SEM analysis of the catalyst a) before and b) after the ECR protocol at the potential of -0.895 V vs. RHE. c,d) IL-SEM analysis of the repeated ECR protocol at -0.975 V vs. RHE, resulting in the formation of new particles (marked in red) besides pre-existing ones (marked in green). e,f) The same experiment as in c,d), however, the gas was exchanged from CO_2 to argon. Green shapes depict particles that grew, while red shapes depict particles that dissolved. g,h) Graphical representation of the proposed mechanism observed in c,d).

Another significant finding in this study was the detection of dissolved Cu species even during CA (**Error! Reference source not found.**g) using inductively coupled plasma mass spectrometry (ICP-MS). Catholyte was sampled at the 59th minute of CA at -0.975 V vs. RHE, while the ECR potential was still applied. A low concentration of Cu species was determined (11.8 ppb). Similarly, another sample was collected during the second ECR protocol, at 59th minute of CA measurement at -0.975 V vs. RHE. Dissolved Cu species were determined in a lower amount (3.7 ppb). This was consistent with the recent report in which Cu was proposed to dissolve through the formation of [Cu^+-ECR intermediates]$_{xH_2O}$ complexes at ECR potential.[19] The ECR selectivity in the first and second CA were not the same (Section S4). Formate production lowered and C-C coupling enhanced indicating that changes in Cu dissolution rate could be connected to ECR selectivity.

Modifications in Cu nanoparticles' morphology were observed in stability experiments over several hours. ECR protocols with varying total CA times, namely 2, 6, and 16 hours, at a potential of -0.975 V vs. RHE, were conducted (Figure 3c-e). Well-defined and smooth Cu nanoparticles, which formed through electrodeposition at the start of CA did not change significantly until 2 hours (Figure 3c). However, anisotropic restructuring of the nanoparticle surface was observed after 6 hours (Figure 3d). Further nanoparticle restructuring occurred until 16 hours of CA (Figure 3e). These three experiments demonstrated the effect of Cu dissolution and subsequent migration, resulting in Cu surface restructuring.

Changes in selectivity for different ECR products were monitored during 16-hour CA as well. Formate production dropped from approximately 22% FE in the first hour to around 3% FE after 6 hours, before increasing back to around 5% FE (Figure 3a). Ethylene formation (and other C_{2+} products, **Error! Reference source not found.**b) increased from 6% to 10% FE and reached a plateau after 4 hours (Figure 3a). At approximately 6 hours, its production started depleting as well. Conversely, a decrease in FE for HER occurred from the start, reaching a minimum before 4 hours. After that, HER FE increase was observed from 6 hours onwards. Methane production in the first hour barely increased and then exhibited a depleting trend (**Error! Reference source not found.**a). However, CO production remained constant throughout the 16-hour experiment (**Error! Reference source not found.**a). A repetition of the 16-hour experiment was conducted for gaseous products, yielding a similar trend (**Error! Reference source not found.**a). By exchanging the electrolyte under potential control (thus preventing catalyst oxidation at OCP and subsequent dissolution), the activity remained unchanged (**Error! Reference source not found.**a). This was a control experiment that eliminated the potential effects of ECR products in the electrolyte, changes in pH throughout the 16 hours, etc., on ECR selectivity. Similar behaviour was observed by Huang et al.[25]

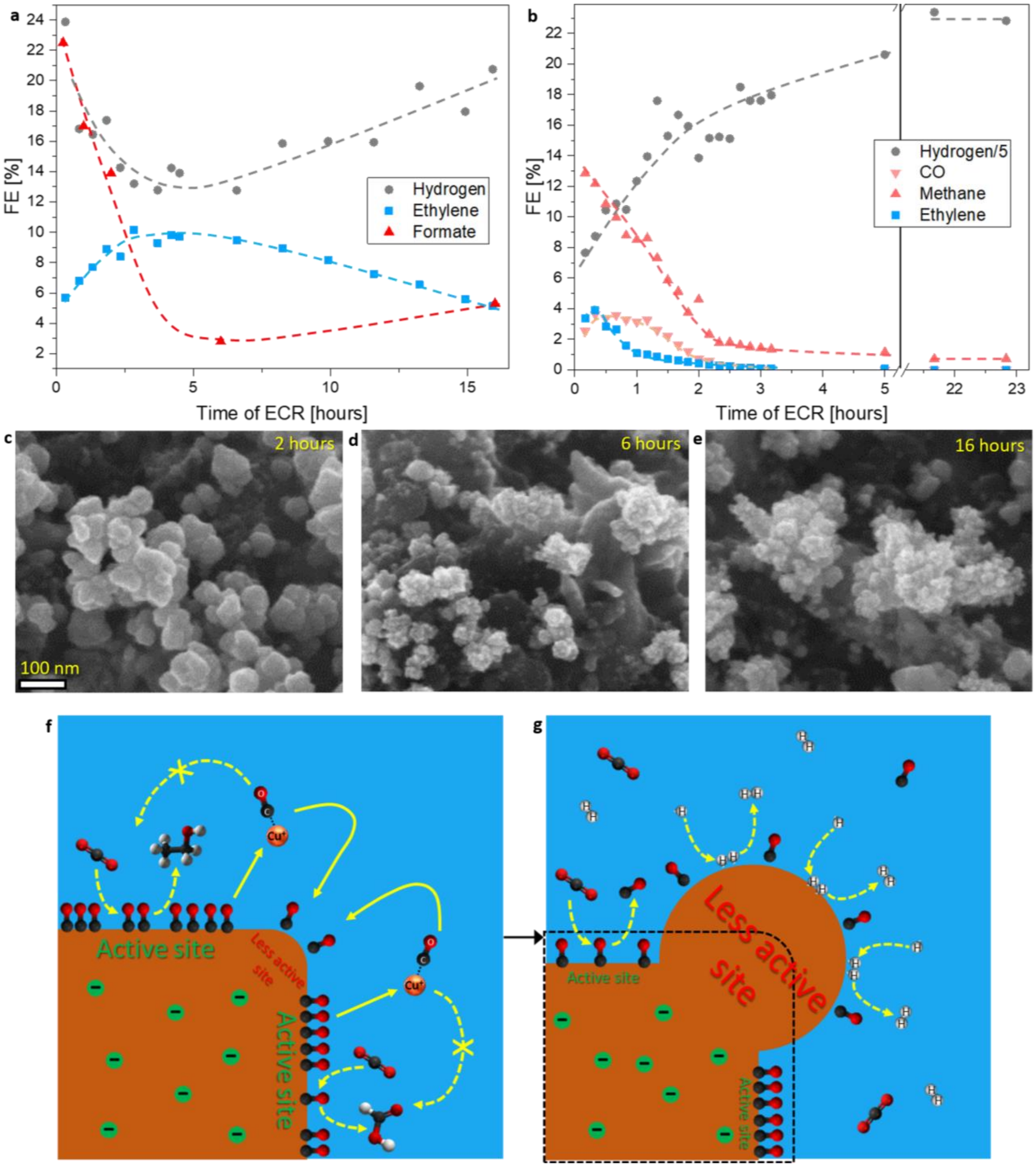

Figure 3. a) Analysis of ECR product selectivity on the first catalyst over a 16-hour CA at a constant potential of -0.975 V vs. RHE for hydrogen, formate, and ethylene FE. b) Analysis of ECR product selectivity changes for gaseous products during a 23-hour CA experiment at a constant potential of -1.0 V vs. RHE conducted on particles formed directly on a GCp. c-e) SEM images of three replicate samples illustrating the first catalyst after varying durations of electrolysis. f) Proposed mechanism depicting dynamic selective dissolution-redeposition of Cu restructuring during CA, leading to g) the formation of hydrogen-producing sites. The shapes of Cu sites are only representative.

Another Cu catalyst was prepared by introducing an electrolyte with dissolved Cu species (Experimental Section) into a cell where the cathode consisted solely of a glassy carbon plate (GCp). The electrodeposition process yielded nanoparticles similar to those observed as reported above, however, with a narrower size distribution (**Error! Reference source not found.**b,c). Formate was not the primary product of the ECR on this catalyst (**Error! Reference source not found.**). A CA stability experiment conducted on this catalyst for 23 hours at -1.000 V vs. RHE potential, yielded a fast ECR deactivation. A decrease in FE for ethylene and methane, accompanied by an increase in FE for hydrogen and CO, was observed from the beginning of the experiment. After one hour FE of CO started decreasing as well leading to overall deactivation. On this catalyst, deactivation occurred at a faster rate compared to Figure 3a, and after 20 hours, practically full deactivation was achieved. The possible effect of Cu leaching from the inner parts of the first catalyst on ECR deactivation was eliminated with this experiment, proving that catalyst deactivation is indeed a general behaviour.

Above mentioned observations confirmed that Cu restructures through dissolution even at ECR potential. We suggest that at these conditions, Cu dissolution via oxidation to Cu^+ occurred by electron transfer to the ECR intermediate. Consequently, the Cu^+ ion became more susceptible to form the soluble complex (**Error! Reference source not found.**). It was demonstrated that Cu restructuring at ECR potential occurs only in the presence of CO_2,[21] therefore, the dissolution of Cu is facilitated by ECR intermediates. In their absence, the presence of Cu^+ species at ECR potential is negligible.[31] Every chemical reaction is a dynamic equilibrium between reactants and products. We propose that dissolution of Cu at ECR potential does not strive from this behaviour, meaning that dynamic dissolution-redeposition mechanism occurred during CA. As shown above (Figure 2), the electrodeposition of dissolved Cu species was facilitated by adsorbed CO_2 reduction intermediates. Dissolved Cu species electrodeposited preferentially to sites with lower coverage with ECR intermediates, presumably the less ECR-active sites.

The dynamic equilibrium between intermediates-mediated dissolution followed by electrodeposition on less-covered sites occurred during CA. Consequently, changes in ECR activity and selectivity over time, leading to deactivation and heightened HER production, can be rationalized. Through multiple iterations of dissolution-redeposition, the less-active ECR sites grew at the expense of the more-active ones (Figure 3f,g). This study intentionally focused on an unstable Cu nanoparticles system to observe this phenomenon, recognizing that different catalysts may exhibit a slower deactivation process. However, by enhancing dissolution, alterations were more pronounced, enabling the determination of the deactivation mechanism during CA.

Stability experiments (Figure 3a,b) and the report presented previously[25] indicated that deactivation did not occur in one step but rather unfolded gradually, potentially triggering the activation of alternative processes. Established ECR mechanisms governing various product pathways involve CO_2 adsorption and reduction to either formate or *CO.[5] From *CO, desired C_{2+} compounds can be produced through an important C-C coupling stage. If this process is inhibited, CO forms through *CO desorption (**Error! Reference source not found.**). The observed CO FE activation after C_{2+} FE deactivation in Figure 3b was a representation of this effect.

The formation of soluble Cu-complexes was more prevalent at formate-producing sites. A decrease in formate production (Section S4) corresponded to a lowered concentration of aqueous Cu species (**Error! Reference source not found.**g). The deactivation of formate-producing sites was faster compared to the deactivation of C-C coupling sites (Figure 3a). The observed activation of C_{2+} products formation in the first 4 hours of ECR on the first catalyst (Figure 3a), could have occurred because more CO_2 became available for *CO on different sites or the formate-producing sites restructured to favour C-C coupling. We propose that the deactivation of original C_{2+} producing sites occurred from the start, however, this process was slower compared to one of the above-mentioned effects, causing the observed activation.

The close interconnection between C-C coupling and HER-producing sites is evident in Figure 3a, where an inverse relationship was observed. When the selectivity for C-C coupling increased, the selectivity for HER decreased, and vice versa. In contrast, interconnection between formate and HER-producing sites was not observed. As mentioned above, C-C coupling requires *CO to be a relatively long-lasting species on the Cu surface, and C_{2+} products involve more than 8 electron transfers. This results in a high population of C_{2+} intermediates on the Cu surface, consequently blocking HER. Similarly, it can be concluded that these sites are more blocked for Cu electrodeposition than formate-producing sites.

The dissolution and formation of presumably $[CuHCOO]_{XH2O}$ complex, like $[Cu_2CO_3]_{5H2O}$ and $[Cu_2C_2O_4]_{4H2O}$,[19] emerged as the predominant step in formate-producing sites deactivation, with redeposition playing a minor role. In contrast, at C-C coupling sites where *CO and other C_{2+} intermediates persisted for longer time periods, dissolution appeared to be less influential, while redeposition was significantly impacted by a high surface coverage. Deactivation mechanism at those two distinct sites is schematically presented in Figure 4.

Further investigations are needed to distinguish the important steps in deactivation for other C_1 and especially individual C_{2+} products, which are particularly important considering their high value. Employing this approach and striving to understand the deactivation mechanisms for different C_{2+} products could benefit future studies in mitigating the deactivation by, for instance, adjusting operational conditions and designing catalysts that would be selective beyond C-C coupling.

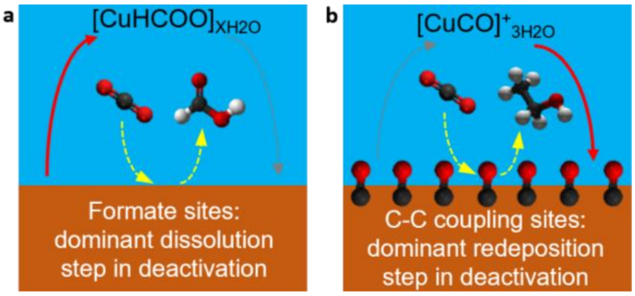

Figure 4. Dominant steps in the dynamic equilibrium of Cu dissolution-redeposition at ECR potential for two distinctive ECR products: a) formate and b) ethylene.

Conclusion

This study showed the dynamic restructuring exhibited by Cu-based catalysts at ECR conditions, a significant challenge in the development of stable, industrially feasible electrocatalysts. The findings demonstrated that the dissolution-redeposition mechanism at the initial stage of ECR played a pivotal role in modifying the morphology of the catalyst. Upon the application of the ECR potential, the electrodeposition of dissolved Cu species was significantly influenced by the ECR. As a result, in these conditions, Cu growth deviated from the common Ostwald ripening mechanism due to Cu surface blockage.

Alterations in Cu surface morphology and ECR selectivity persisted even during CA, at applied ECR potential. The detection of dissolved Cu species indicated the formation of $[Cu^+$-ECR intermediates$]_{xH_2O}$ complexes under these conditions. The dynamic equilibrium of dissolution-redeposition at ECR potential, facilitated Cu migration to the less active sites, due to their lower occupancy by ECR intermediates. Iterative cycles of this process led to the complete deactivation of the Cu catalyst, shifting ECR selectivity towards the HER.

We anticipate that our findings and methodologies will inform future endeavours aimed at designing stable catalysts capable of effectively closing humanity's CO_2 cycle. The observed restructuring phenomena for other metals indicate broader implications of this knowledge beyond Cu.[32,33] In conclusion, we echo the sentiment encapsulated in the following quote summarising this work: "*Copper's most powerful tool for fighting global warming is also its greatest weakness.*"

Supporting Information

The authors have cited additional references within the Supporting Information.[34–53]

Acknowledgments

The authors would like to acknowledge the Slovenian Research and Innovation Agency (ARIS) programs P2-0393, P2-0118, P1-0242 and I0-0003; the projects N2-0155, N2-0337, J1-4401, J2-50076 and J7-4638. M.A.N. acknowledges the funding for Marie Skłodowska-Curie Actions, Individual Fellowships, project CO2-CAT-ALOG (grant reference no. 897866) from the EU commission for Horizon 2020 Framework Programme. The project is co-financed by the Republic of Slovenia, the Ministry of Higher Education, Science and Innovation, and the European Union under the European Regional Development Fund. A.R.K. would like to acknowledge the support of the Milan Lenarčič Foundation and the Janko Jamnik Doctoral Scholarship.

Keywords: Carbon Dioxide • Copper • Dissolution-Redeposition • Dynamic Equilibrium • Electrochemistry

[1] Scripps Institution of Oceanography at UC San Diego, "The Keeling Curve," can be found under https://keelingcurve.ucsd.edu/, **2024** (accessed 26 March 2024).
[2] European Commission, "Factsheets on the European Green Deal," can be found under https://commission.europa.eu/publications/factsheets-european-green-deal_en, **2019** (accessed 26 March 2024).
[3] European Commission, "Delivering the European Green Deal," can be found under https://commission.europa.eu/publications/delivering-european-green-deal_en, **2021** (accessed 26 March 2024).
[4] R. S. Haszeldine, S. Flude, G. Johnson, V. Scott, *Philos. Trans. A Math. Phys. Eng. Sci.* **2018**, *376*, 20160447.
[5] S. Nitopi, E. Bertheussen, S. B. Scott, X. Liu, A. K. Engstfeld, S. Horch, B. Seger, I. E. L. Stephens, K. Chan, C. Hahn, J. K. Nørskov, T. F. Jaramillo, I. Chorkendorff, *Chem. Rev.* **2019**, *119*, 7610–7672.
[6] X. Chen, Y. Zhao, J. Han, Y. Bu, *Chempluschem* **2023**, *88*, DOI 10.1002/cplu.202200370.
[7] K. J. P. Schouten, Y. Kwon, C. J. M. Van Der Ham, Z. Qin, M. T. M. Koper, *Chem. Sci.* **2011**, *2*, 1902–1909.
[8] Y. Huang, A. D. Handoko, P. Hirunsit, B. S. Yeo, *ACS Catal.* **2017**, *7*, 1749–1756.
[9] C. Hahn, T. Hatsukade, Y. G. Kim, A. Vailionis, J. H. Baricuatro, D. C. Higgins, S. A. Nitopi, M. P. Soriaga, T. F. Jaramillo, *Proc. Natl. Acad. Sci.* **2017**, *114*, 5918–5923.
[10] G. L. De Gregorio, T. Burdyny, A. Loiudice, P. Iyengar, W. A. Smith, R. Buonsanti, *ACS Catal.* **2020**, *10*, 4854–4862.
[11] R. Reske, H. Mistry, F. Behafarid, B. Roldan Cuenya, P. Strasser, *J. Am. Chem. Soc.* **2014**, *136*, 6978–6986.
[12] D. Kim, C. S. Kley, Y. Li, P. Yang, *Proc. Natl. Acad. Sci.* **2017**, *114*, 10560–10565.
[13] K. Manthiram, B. J. Beberwyck, A. P. Alivisatos, *J. Am. Chem. Soc.* **2014**, *136*, 13319–13325.
[14] G. H. Simon, C. S. Kley, B. Roldan Cuenya, *Angew. Chem. Int. Ed.* **2021**, *60*, 2561–2568.
[15] S. Popović, M. Smiljanić, P. Jovanovič, J. Vavra, R. Buonsanti, N. Hodnik, *Angew. Chem. Int. Ed.* **2020**, *59*, 14736–14746.
[16] S. Popovic, M. Bele, N. Hodnik, *ChemElectroChem* **2021**, *8*, 2634–2639.
[17] F. D. Speck, S. Cherevko, *Electrochem. Commun.* **2020**, *115*, DOI 10.1016/j.elecom.2020.106739.
[18] J. Vavra, T. H. Shen, D. Stoian, V. Tileli, R. Buonsanti, *Angew. Chem. Int. Ed.* **2021**, *60*, 1347–1354.
[19] J. Vavra, G. P. L. Ramona, F. Dattila, A. Kormányos, T. Priamushko, P. P. Albertini, A. Loiudice, S. Cherevko, N. Lopéz, R. Buonsanti, *Nat. Catal.* **2024**, *7*, 89–97.
[20] S. J. Raaijman, N. Arulmozhi, M. T. M. Koper, *ACS Appl. Mater. Interfaces* **2021**, *13*, 48730–48744.
[21] S. H. Lee, J. C. Lin, M. Farmand, A. T. Landers, J. T. Feaster, J. E. Avilés Acosta, J. W. Beeman, Y. Ye, J. Yano, A. Mehta, R. C. Davis, T. F. Jaramillo, C. Hahn, W. S. Drisdell, *J. Am. Chem. Soc.* **2021**, *143*, 588–592.
[22] Y. G. Kim, J. H. Baricuatro, A. Javier, J. M. Gregoire, M. P. Soriaga, *Langmuir* **2014**, *30*, 15053–15056.
[23] P. Grosse, D. Gao, F. Scholten, I. Sinev, H. Mistry, B. Roldan Cuenya, *Angew. Chem. Int. Ed.* **2018**, *57*, 6192–6197.
[24] P. Grosse, A. Yoon, C. Rettenmaier, A. Herzog, S. W. Chee, B. Roldan Cuenya, *Nat. Commun.* **2021**, *12*, DOI 10.1038/s41467-021-26743-5.
[25] J. Huang, N. Hörmann, E. Oveisi, A. Loiudice, G. L. De Gregorio, O. Andreussi, N. Marzari, R. Buonsanti, *Nat. Commun.* **2018**, *9*, DOI 10.1038/s41467-018-05544-3.
[26] T. H. Phan, K. Banjac, F. P. Cometto, F. Dattila, R. García-Muelas, S. J. Raaijman, C. Ye, M. T. M. Koper, N. López, M. Lingenfelder, *Nano Lett.* **2021**, *21*, 2059–2065.

[27] H. Jung, S. Y. Lee, C. W. Lee, M. K. Cho, D. H. Won, C. Kim, H. S. Oh, B. K. Min, Y. J. Hwang, *J Am Chem Soc* **2019**, *141*, 4624–4633.

[28] C. M. Gunathunge, X. Li, J. Li, R. P. Hicks, V. J. Ovalle, M. M. Waegele, *J. Phys. Chem. C* **2017**, *121*, 12337–12344.

[29] W. T. Osowiecki, J. J. Nussbaum, G. A. Kamat, G. Katsoukis, M. Ledendecker, H. Frei, A. T. Bell, A. P. Alivisatos, *ACS Appl. Energy Mater.* **2019**, *2*, 7744–7749.

[30] B. Eren, D. Zherebetskyy, L. L. Patera, C. H. Wu, H. Bluhm, C. Africh, L.-W. Wang, G. A. Somorjai, M. Salmeron, *Science (1979)* **2016**, *351*, 475–478.

[31] Marcel Pourbaix, *Atlas of Electrochemical Equilibria in Aqueous Solutions*, NACE International, Houston, CEBELCOR, Brussels, **1966**, pp. 384-392.

[32] F. Li, X. V. Medvedeva, J. J. Medvedev, E. Khairullina, H. Engelhardt, S. Chandrasekar, Y. Guo, J. Jin, A. Lee, H. Thérien-Aubin, A. Ahmed, Y. Pang, A. Klinkova, *Nat. Catal.* **2021**, *4*, 479–487.

[33] D. Y. Chung, P. P. Lopes, P. Farinazzo Bergamo Dias Martins, H. He, T. Kawaguchi, P. Zapol, H. You, D. Tripkovic, D. Strmcnik, Y. Zhu, S. Seifert, S. Lee, V. R. Stamenkovic, N. M. Markovic, *Nat. Energy* **2020**, *5*, 222–230.

[34] N. Sreekanth, K. L. Phani, *Chem. Commun.* **2014**, *50*, 11143–11146.

[35] C. Schneider, W. Rasband, K. Eliceiri, *Nat. Methods* **2012**, *9*, 671–675.

[36] Y. Li, F. Cui, M. B. Ross, D. Kim, Y. Sun, P. Yang, *Nano Lett.* **2017**, *17*, 1312–1317.

[37] N. Sreekanth, M. A. Nazrulla, T. V. Vineesh, K. Sailaja, K. L. Phani, *Chem. Commun.* **2015**, *51*, 16061–16064.

[38] S. Liu, H. Yang, X. Su, J. Ding, Q. Mao, Y. Huang, T. Zhang, B. Liu, *J. Energy Chem.* **2019**, *36*, 95–105.

[39] R. D. Kent, P. J. Vikesland, *Environ. Sci. Technol.* **2016**, *50*, 6772–6781.

[40] Y. Li, D. Kim, S. Louisia, C. Xie, Q. Kong, S. Yu, T. Lin, S. Aloni, S. C. Fakra, P. Yang, *Proc. Natl. Acad. Sci.* **2020**, *117*, 9194–9201.

[41] Y. Yang, S. Louisia, S. Yu, J. Jin, I. Roh, C. Chen, M. V. Fonseca Guzman, J. Feijóo, P. C. Chen, H. Wang, C. J. Pollock, X. Huang, Y. T. Shao, C. Wang, D. A. Muller, H. D. Abruña, P. Yang, *Nature* **2023**, *614*, 262–269.

[42] N. Hodnik, M. Zorko, M. Bele, S. Hočevar, M. Gaberšček, *Journal of Physical Chemistry C* **2012**, *116*, 21326–21333.

[43] S. Popović, M. A. Nazrulla, P. Šket, K. M. Kamal, B. Likozar, L. Suhadolnik, L. Pavko, A. K. Surca, M. Bele, N. Hodnik, *Electrochim. Acta* **2022**, *436*, 141458.

[44] N. Hodnik, M. Zorko, B. Jozinović, M. Bele, G. Dražič, S. Hočevar, M. Gaberšček, *Electrochem. Commun.* **2013**, *30*, 75–78.

[45] M. Zorko, B. Jozinović, M. Bele, N. Hodnik, M. Gaberšček, *Ultramicroscopy* **2014**, *140*, 44–50.

[46] J. J. Velasco-Velez, J. J. Velasco-Velez, R. V. Mom, L. E. Sandoval-Diaz, L. J. Falling, C. H. Chuang, D. Gao, D. Gao, T. E. Jones, Q. Zhu, Q. Zhu, R. Arrigo, B. Roldan Cuenya, A. Knop-Gericke, A. Knop-Gericke, T. Lunkenbein, R. Schlögl, R. Schlögl, *ACS Energy Lett.* **2020**, *5*, 2106–2111.

[47] Y. Lum, J. W. Ager, *Angew. Chem. Int. Ed.* **2018**, *57*, 551–554.

[48] P. De Luna, R. Quintero-Bermudez, C. T. DInh, M. B. Ross, O. S. Bushuyev, P. Todorović, T. Regier, S. O. Kelley, P. Yang, E. H. Sargent, *Nat. Catal.* **2018**, *1*, 103–110.

[49] H. F. Goldstein, D.-S. Kim, P. Y. Yu, L. C. Bournet, J.-P. Chaminade, L. Nganga, *Phys. Rev. B* **1990**, *41*, 7192–7194.

[50] X. K. Chen, J. C. Irwin, J. P. Franck, *Phys. Rev. B* **1995**, *52*, R13 130-R13 133.

[51] J. Chrzanowski, J. C. Irwin, *Solid State Commun.* **1989**, *70*, 11–14.

[52] L. Debbichi, M. C. Marco De Lucas, J. F. Pierson, P. Krüger, *J. Phy. Chem. C* **2012**, *116*, 10232–10237.

[53] Y. Deng, A. D. Handoko, Y. Du, S. Xi, B. S. Yeo, *ACS Catal.* **2016**, *6*, 2473–2481.

Entry for the Table of Contents

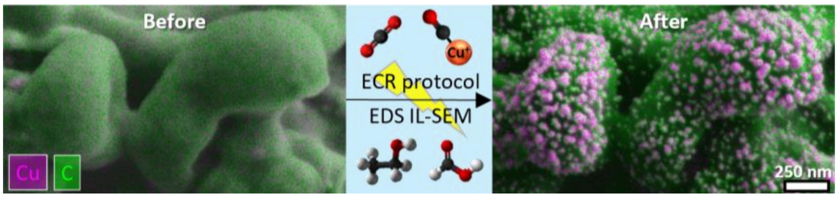

Copper dissolution-redeposition significantly transforms catalysts at the initiation of electrochemical CO_2 reduction, with restructuring persisting even at reaction conditions where CO_2 reduction intermediates mediate a dynamic equilibrium between dissolved and deposited copper, gradually resulting in catalyst deactivation during long-term operation.

@Electrocatalyst